machines

MDPI

Article

Perfect Tracking Control of Linear Sliders Using Sliding Mode Control with Uncertainty Estimation Mechanism

Tomoya Hoshina, Takato Yamada and Mingcong Deng *

Department of Electrical and Electronic Engineering, Graduate School of Engineering, Tokyo University of Agriculture and Technology, 2-24-16 Nakacho, Koganei-shi 184-8588, Tokyo, Japan; s239681t@st.go.tuat.ac.jp (T.H.)

* Correspondence: deng@cc.tuat.ac.jp

Abstract: This paper aims to achieve precise position control of a stage used in semiconductor exposure apparatus. The demand for smart devices, such as smartphones, is rapidly expanding, and their performance is expected to continue to improve. To manufacture these devices, it is necessary to miniaturize semiconductor devices and improve productivity. The precise control of semiconductor exposure apparatus is important for the manufacture of ultra-small semiconductor devices. The stage of semiconductor exposure apparatus uses a linear motor, and this paper performs high-precision perfect tracking control of this stage. Perfect tracking control is a control method that always follows the command value while the command value changes moment by moment, and requires high accuracy. In high-precision positioning, uncertainty in the stage model has a significant impact. Therefore, this paper proposes a method to reduce tracking errors due to the influence of uncertainty by performing uncertainty compensation using sliding mode control with the estimated value of uncertainty. The estimation of uncertainty uses a method that combines Kernel LMS with an observer. Instead of the widely used Gaussian kernel, this paper uses a generalized Gaussian kernel that allows for finer parameter settings. Furthermore, this paper proposes a method to adaptively optimize the shape parameter of the generalized Gaussian kernel. Our simulations and experiments confirm that the proposed method improves tracking performance compared to conventional sliding mode control.

Keywords: sliding mode control; adaptive identification; semiconductor manufacturing; uncertainty compensation; Kernel LMS; perfect tracking control

check for updates

Citation: Hoshina, T.; Yamada, T.; Deng, M. Perfect Tracking Control of Linear Sliders Using Sliding Mode Control with Uncertainty Estimation Mechanism. *Machines* **2024**, *12*, 212. https://doi.org/10.3390/machines12040212

Academic Editor: Junyong Zhai

Received: 20 February 2024
Revised: 15 March 2024
Accepted: 20 March 2024
Published: 22 March 2024

Copyright: © 2024 by the authors. Licensee MDPI, Basel, Switzerland. This article is an open access article distributed under the terms and conditions of the Creative Commons Attribution (CC BY) license (https://creativecommons.org/licenses/by/4.0/).

1. Introduction

Currently, attention is focused on the advancement of the IoT society worldwide. Specifically, smartphones and smart home appliances are examples of such devices. In the near future, fully automated vehicles and contact lenses that perform the same functions as smartphones by simply being worn on the eyes are expected to appear. Since semiconductor devices are the foundation of these devices, it is expected that semiconductor device manufacturing technology will become increasingly important. Therefore, various studies have been conducted in different fields to meet the manufacturing requirements of semiconductor devices [1–7].

This paper aims to achieve high-precision positioning of the exposure stage used in semiconductor manufacturing. To achieve high-precision positioning of the stage, a precise mathematical model that accurately represents the dynamic characteristics of the stage is required. However, due to the nonlinearity and disturbance effects on the dynamic characteristics of the stage, it is difficult to construct a precise mathematical model, and its performance is degraded due to the influence of unconsidered uncertainties. Therefore, in order to achieve high-precision positioning of the stage, it is necessary to construct a control system that takes into account the influence of uncertainties. Two methods have been proposed for constructing control systems that consider uncertainties. The first

method enhances the robustness of the controller against uncertainties to compensate for instability under conditions that include uncertainties [8–12]. The second method involves estimating uncertainties and model parameters and modifying the control input based on the estimated values [13–16]. The first method focuses on stability and does not consider improving control performance, making it unsuitable for high-precision control. Therefore, in this paper, the second method is used to identify uncertainties and modify the control input based on the identification results. In particular, sequential identification of uncertainties is performed to cope with rapidly changing uncertainties. There have been studies on sequential model identification, such as [17–21], and their effectiveness has been confirmed.

Previous studies have proposed a control method based on operator theory for constructing a mathematical model that represents the dynamic characteristics of the stage, focusing on the linear motor's chain of magnetic flux [22]. Operator theory is a control theory that represents the input–output characteristics of the plant using a nonlinear mapping method called an operator. This design method does not require the state variables of the plant and is easy to implement. It has been proposed for various applications, such as wireless power transmission, processes, and nano materials, as it does not require a special form for nonlinearity [23–26]. However, previous studies did not consider the influence of uncertainties, resulting in significant discrepancies between simulation results and experimental results. Additionally, control methods using model estimation by AI have been proposed [27–29]. Research on stage positioning using air pressure has also been conducted [30–32]. In both methods, even if uncertainty compensation is performed, it is difficult to adapt to changes in uncertainties because the uncertainty model is identified offline or learning is performed at long intervals. In this paper, sequential identification of uncertainty models is performed using Kernel LMS [33] and an optimal observer, and uncertainty compensation is performed using the identified uncertainty model and sliding mode control [34–37]. Kernel LMS is a method that can adaptively identify nonlinear functions by approximating them using the kernel method, and it is widely used in the field of signal processing [38–41]. There are other methods for identifying nonlinear functions, such as Neural Networks (NNs) [42–44] and Support Vector Machines (SVMs) [45–47], but they have high learning costs and cannot easily achieve adaptive identification. On the other hand, Kernel LMS has the advantage of low learning costs and the ability to achieve adaptive identification. Research applying Kernel LMS to control has been conducted, such as in [48,49], and its ability to handle complex signals such as drones and active noise cancellation has been confirmed. Many methods using various kernels, including Gaussian kernels, have been proposed, but in this paper, identification is performed using a generalized Gaussian kernel based on generalized Gaussian distribution [50,51]. Furthermore, the shape parameter included in the kernel is sequentially optimized to identify the optimal kernel.

This paper is structured as follows. In Section 2, the equipment used in the experiments is described. In Section 3, the problem formulation is presented. In Section 4, the derivation of the stage model is described. In Section 5, the proposed method for the controller is presented. In Section 6, the effectiveness of the proposed method is verified through simulations and experiments. In Section 7, the paper is summarized.

2. Experimental System

Figures 1 and 2 depict a photograph and a schematic diagram, respectively, of the experimental apparatus employed in this study. The plant consists of a linear motor stage connected to an air slider via bolts, with the stage made to float and friction eliminated by supplying compressed air to the air slider. By applying an electric current to the linear motor, the stage can slide left and right. The position of the stage is observed using a laser sensor attached to the device, and a position signal is sent to the DSP. The DSP processes the position signal and inputs the resulting input voltage signal to the driver circuit, thereby controlling the linear motor by applying a current to it.

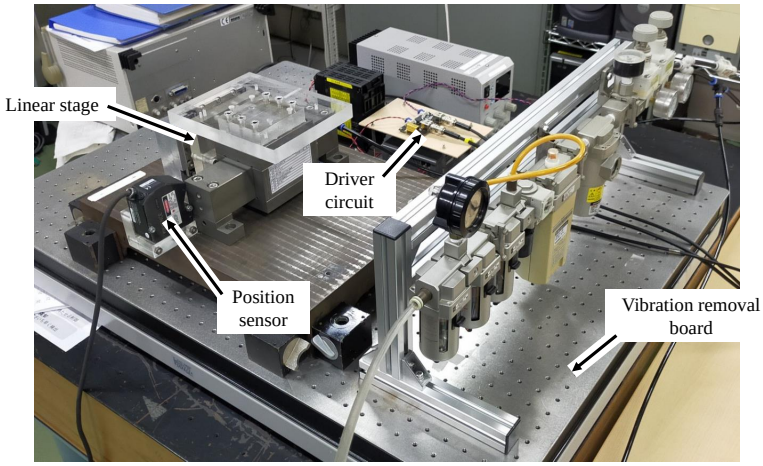

Figure 1. Photograph of the experimental apparatus.

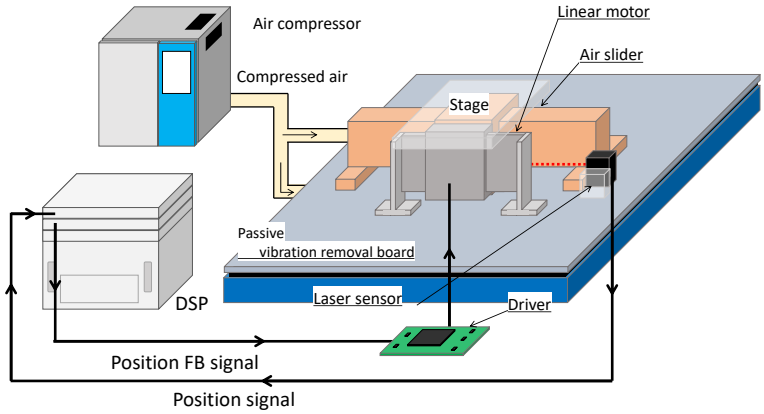

Figure 2. Schematic diagram of the experimental apparatus.

3. Problem Statement

The kinetic model of the linear stage P is represented by Equation (1), where $y \in Y$ denotes the stage position, $m > 0$ is the mass of the slider, $f : Y \times V \to F$ is the nonlinear external force applied to the stage, and $f_u \in F$ is the manipulated variable.

$$P : F \to Y : m\ddot{y}(t) = f(y, \dot{y})(t) + f_u(t) \tag{1}$$

Let the operator f be decomposed into a known linear operator f_0 and an unknown bounded nonlinear uncertainty operator Δ, as shown in Equation (2).

$$f(y, \dot{y}) = f_0(y, \dot{y}) + \Delta(y, \dot{y}) \tag{2}$$

It is assumed that the following conditions hold for uncertainty Δ.

Assumption 1. *Δ is a bounded operator: For any bounded $y \in Y$ and $\dot{y} \in V$, $\Delta(y, \dot{y}) < \infty$ holds. If this assumption is not satisfied, it is impossible to output a manipulated variable that eliminates the estimated uncertainty Δ.*

Assumption 2. *Δ is sufficiently small compared to f_0: For any bounded $y \in Y$ and $\dot{y} \in V$, $\Delta(y, \dot{y}) \ll f_0(y, \dot{y})$ holds. Under this assumption, the influence of uncertainty can be reduced by making the estimation error sufficiently small.*

Assumption 3. *The upper limit of the second-order differential value of* Δ *is known: For any bounded* $y \in Y$ *and* $\dot{y} \in V$, $\left|\frac{\mathrm{d}^2\Delta}{\mathrm{d}t^2}(y,\dot{y})\right| \leq \bar{\Delta}^{(2)}$ *holds. Under this assumption, it is possible to stabilize the plant by suppressing the upper limit* $\bar{\Delta}^{(2)}$.

Furthermore, the ideal model P_n is defined as shown in Equation (3) using the above f_0, and the difference from the actual model is defined as shown in Equation (4), where $y^* \in Y$ is the ideal position of the stage, and $f_u^* \in F$ is the ideal manipulated variable.

$$P_n : F \to Y : m\ddot{y}^*(t) = f_0(y^*, \dot{y}^*)(t) + f_u^*(t) \tag{3}$$

$$e(t) = y(t) - y^*(t) \tag{4}$$

The dynamics of e are expressed as follows:

$$\begin{aligned} \ddot{e}(t) &= \ddot{y}(t) - \ddot{y}^*(t) \\ &= \frac{1}{m}(f_0(e,\dot{e})(t) + \Delta(y,\dot{y})(t) + f_u(t) - f_u^*(t)) \end{aligned} \tag{5}$$

In this paper, a control system that ensures $e \to 0$ using a kernel adaptive filter to eliminate uncertainty Δ is proposed. Furthermore, it achieves perfect tracking to a continuous set point r by employing sliding mode control with an integral term.

In this paper, we adopt two notations for the differential quantity of a given state x, $\dot{x}$ and $x^{(n)}$, with $\ddot{x}$ representing the second-order differential and $x^{(n)}$ the higher-order cases. That is, $\ddot{x} = x^{(2)} = \frac{\mathrm{d}^2 x}{\mathrm{d}t^2}$.

4. Model

In this paper, an improved version of the model from [22] is used as the model for the plant, which is represented below:

$$m\ddot{y}(t) = -c\dot{y}(t) + \Phi(y)i(t) - W'(y)(t) \tag{6}$$

$$L\dot{i}(t) = -Ri(t) - \Phi(y)\dot{y}(t) + u(t) \tag{7}$$

$$\Phi(y) = \hat{a} - \hat{b}\Big(\cosh(\hat{k}y) - 1\Big) \tag{8}$$

$$W'(y) = \frac{L_x L_z\Big(\mu_0 - \mu_f\Big)}{2\mu_0\mu_f}\left(-\hat{b}^2\sinh\Big(\hat{k}l_y\Big)\sinh\Big(2\hat{k}y\Big) + 4\Big(\hat{a}\hat{b} + \hat{b}^2\Big)\sinh\left(\frac{\hat{k}}{2}l_y\right)\sinh\Big(\hat{k}y\Big)\right) \tag{9}$$

where $c > 0$ is the velocity resistance of the stage, $\Phi(\cdot)$ is the operator representing the magnetic flux crossing the coil of the linear motor, $W'(\cdot)$ is the operator representing the force due to the magnetic potential of the linear motor, $L > 0$ is the inductance of the linear motor, $R > 0$ is the electrical resistance of the linear motor, $\hat{a} > 0$, $\hat{b} > 0$, and $\hat{k} > 0$ are the parameters of the magnetic flux, and $\mu_0 > 0$ and $\mu_f > 0$ are the permeability of the vacuum and the coil, respectively. $L_x > 0$ and $L_z > 0$ are the lengths of the linear motor in each axis direction, and $l_y > 0$ is the length of the coil in the y axis direction, and these parameters correspond to the structure of the linear motor shown in Figure 3.

This chapter describes the derivation of this model.

Derivation of the Model

This model considers the spring-like characteristics caused by the permanent magnet of the linear motor. Due to its structural features, the linear motor exerts a force that tries to slide the stage position towards the center based on the gradient of the magnetic potential of the permanent magnet. A conceptual diagram is shown in Figure 3.

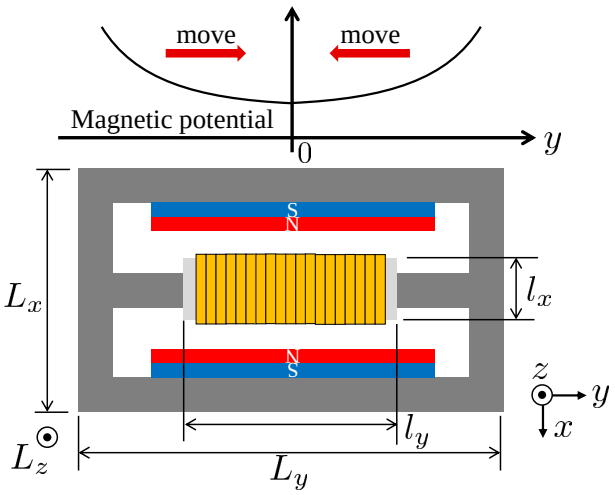

Figure 3. Structure of the linear motor.

The magnetic energy per unit volume ϕ is represented by Equation (10) using the magnetic flux density Φ:

$$\phi = \frac{1}{2\mu}\Phi^2 \tag{10}$$

where μ is the magnetic permeability. Assuming that the magnetic flux density in the regions with and without coils in Figure 3 is constant in the x and z directions, the total magnetic energy W of the linear motor is represented by Equation (11):

$$W(y) = L_x L_z \frac{1}{2\mu_0} \int_{-\frac{L_y}{2}}^{\frac{L_y}{2}} \Phi^2(y)\mathrm{d}y + l_x L_z \left(\frac{1}{2\mu_f} - \frac{1}{2\mu_0}\right) \int_{-\frac{l_y}{2}+y}^{\frac{l_y}{2}+y} \Phi^2(y)\mathrm{d}y \tag{11}$$

where L_x, L_y, and L_z are the lengths of the linear motor in the x, y, and z directions, and l_x and l_y are the lengths of the coil in the x and y directions, respectively. The first term of this equation represents the total magnetic energy when the coil is not present, and the second term represents the change in magnetic energy when the coil is added. When the coil is not present, the permeability of the entire region is μ_0, so the entire region is integrated as in the first term. When the coil is present, the region of $l_x \times l_y$ is replaced by the coil, so the region of the coil $l_x \times l_y$ is integrated as in the second term. By substituting Equation (8) into Equations (11) and (12), we obtain

$$\begin{aligned} W(y) = {} & \frac{L_x L_z}{2\mu_0}\left(\hat{a}^2 + 2\hat{a}\hat{b} + \frac{3}{2}\hat{b}^2\right)\left(L_y - l_y + \frac{\mu_0}{\mu_f} l_y\right) \\ & + \frac{L_x L_z}{4\mu_0 \hat{k}}\left(\hat{b}^2 \sinh\left(\hat{k}L_y\right) - 8\left(\hat{a}\hat{b} + \hat{b}^2\right)\sinh\left(\frac{\hat{k}}{2}L_y\right)\right) \\ & + \frac{L_x L_z\left(\mu_0 - \mu_f\right)}{4\mu_0\mu_f \hat{k}}\left(\hat{b}^2 \sinh\left(\hat{k}l_y\right)\cosh\left(2\hat{k}y\right) - 8\left(\hat{a}\hat{b} + \hat{b}^2\right)\sinh\left(\frac{\hat{k}}{2}l_y\right)\cosh\left(\hat{k}y\right)\right) \end{aligned} \tag{12}$$

By differentiating Equation (12) with respect to y, the force due to the total magnetic energy of the linear motor W' in Equation (9) is obtained.

5. Proposed Control Method

This chapter describes a method for estimating uncertainty using a kernel adaptive filter and perfect tracking control with sliding mode control, which is proposed in this paper.

5.1. Uncertainty Estimation

The estimated value of uncertainty $\hat{\Delta}$ is expressed by using the model with kernel regression, as shown in Equations (13)–(16):

$$\hat{\Delta}(t) = \hat{\boldsymbol{w}}(t)^T \boldsymbol{k}(\boldsymbol{x}(t)) \tag{13}$$

$$\boldsymbol{k}(\boldsymbol{x}(t)) = \begin{pmatrix} \kappa(\boldsymbol{x}(t), \tilde{\boldsymbol{x}}_1) & \cdots & \kappa(\boldsymbol{x}(t), \tilde{\boldsymbol{x}}_N) \end{pmatrix}^T \tag{14}$$

$$\kappa(\boldsymbol{x}, \tilde{\boldsymbol{x}}) = \exp\left(-\left(\frac{g(\gamma)\|\boldsymbol{x} - \tilde{\boldsymbol{x}}\|}{\sigma} \right)^{\gamma} \right) \tag{15}$$

$$g(\gamma) = \sqrt{\frac{\Gamma(3/\gamma)}{\Gamma(1/\gamma)}} \tag{16}$$

where $\boldsymbol{x} = \begin{pmatrix} y & \dot{y} \end{pmatrix}^T$ is the state variable of the plant, $\hat{\boldsymbol{w}} \in \mathbb{R}^N$ is the adaptive weight vector of the model, and $\boldsymbol{k}(\cdot) : \mathbb{R}^2 \to \mathbb{R}^N$ is the kernel function vector. In this paper, $\boldsymbol{k}$ uses the generalized Gaussian kernel expressed by Equations (15) and (16), where $\tilde{\boldsymbol{x}}_i \in \mathbb{R}^2$ represents the learning data, $\sigma > 0$ is the standard deviation of the kernel, $\gamma > 0$ is the order of the norm, and $\Gamma(\cdot)$ is the gamma function.

The estimation error ε of uncertainty is defined as shown in Equation (17).

$$\begin{aligned} \varepsilon(t) &= \Delta(t) - \hat{\Delta}(t) \\ &= \Delta(t) - \hat{\boldsymbol{w}}(t)^T \boldsymbol{k}(\boldsymbol{x})(t) \end{aligned} \tag{17}$$

In order to minimize ε, an observer based on the evaluation function J shown in Equations (18) and (19) is considered, where $\hat{\cdot}$ represents the estimated values of each variable, $P = \mathrm{diag}(p_y, 1), p_y > 0$ is the weight for the state variable, and $p_\varepsilon > 0$ is the weight for the uncertainty estimation error.

$$J(\hat{\boldsymbol{w}}) = \frac{1}{2}\left((\boldsymbol{x} - \hat{\boldsymbol{x}})^T P (\boldsymbol{x} - \hat{\boldsymbol{x}}) + p_\varepsilon \varepsilon^2 \right) \tag{18}$$

$$\hat{\boldsymbol{x}}(t) = \begin{pmatrix} \hat{y}(t) & \hat{\dot{y}}(t) \end{pmatrix}^T \tag{19}$$

The observer is designed as shown in Equation (20), where v_1, v_2, and $\boldsymbol{v}_3$are the state correction inputs of the observer.

$$\frac{\mathrm{d}}{\mathrm{d}t}\begin{pmatrix} \hat{y} \\ \hat{\dot{y}} \\ \hat{\boldsymbol{w}} \end{pmatrix}(t) = \begin{pmatrix} \hat{\dot{y}}(t) + v_1(t) \\ \frac{1}{m}\left\{ f_0(\hat{y}, \hat{\dot{y}})(t) + \hat{\Delta}(t) + f_u(t) \right\} + v_2(t) \\ \boldsymbol{v}_3(t) \end{pmatrix} \tag{20}$$

To adaptively minimize the evaluation function shown in Equation (18), it is desirable for it to be a Lyapunov function. Therefore, let us consider the time derivative of it.

$$\dot{J}(\hat{\boldsymbol{w}}) = (\boldsymbol{x} - \hat{\boldsymbol{x}})^T P (\dot{\boldsymbol{x}} - \dot{\hat{\boldsymbol{x}}}) + p_\varepsilon \varepsilon \dot{\varepsilon} \tag{21}$$

By substituting Equations (1), (17), and (20) into Equation (21), Equation (22) is expressed.

$$\begin{aligned}\dot{J}(\hat{\boldsymbol{w}}) &= (y-\hat{y})p_y(\dot{y}-\hat{\dot{y}}-v_1)\\ &\quad+(\dot{y}-\hat{\dot{y}})\frac{1}{m}(f_0(y-\hat{y},\dot{y}-\hat{\dot{y}})+\varepsilon-mv_2)\\ &\quad+p_\varepsilon\varepsilon\left(\dot{\Delta}-\hat{\boldsymbol{w}}^T\dot{\boldsymbol{k}}(\boldsymbol{x})-\boldsymbol{v}_3^T\boldsymbol{k}(\boldsymbol{x})\right)\\ &= -p_y(y-\hat{y})v_1\\ &\quad+(\dot{y}-\hat{\dot{y}})\left\{p_y(y-\hat{y})+\frac{1}{m}(f_0(y-\hat{y},\dot{y}-\hat{\dot{y}}))-v_2\right\}\\ &\quad+\varepsilon\left\{\frac{1}{m}(\dot{y}-\hat{\dot{y}})+p_\varepsilon\left(\dot{\Delta}-\hat{\boldsymbol{w}}^T\dot{\boldsymbol{k}}(\boldsymbol{x})\right)-p_\varepsilon\boldsymbol{v}_3^T\boldsymbol{k}(\boldsymbol{x})\right\}\end{aligned} \tag{22}$$

In order to make the first and second terms of Equation (22) negative and the third term sufficiently small, v_1, v_2, and $\boldsymbol{v}_3$ are designed as shown in Equations (23)–(25), where $G_1 > 0$ and $G_2 > 0$ are design parameters.

$$v_1 = G_1(y-\hat{y}) \tag{23}$$

$$v_2 = p_y(y-\hat{y})+\frac{1}{m}f_0(y-\hat{y},\dot{y}-\hat{\dot{y}})+G_2(\dot{y}-\hat{\dot{y}}) \tag{24}$$

$$\boldsymbol{v}_3 = \frac{\boldsymbol{k}(\boldsymbol{x})}{mp_\varepsilon\|\boldsymbol{k}(\boldsymbol{x})\|^2}(\dot{y}-\hat{\dot{y}}) \tag{25}$$

By substituting Equations (23)–(25) into Equation (22), Equation (26) is expressed.

$$\dot{J}(\hat{\boldsymbol{w}}) = -G_1(y-\hat{y})^2-G_2(\dot{y}-\hat{\dot{y}})^2+p_\varepsilon\varepsilon\left(\dot{\Delta}-\hat{\boldsymbol{w}}^T\dot{\boldsymbol{k}}(\boldsymbol{x})\right) \tag{26}$$

Since p_ε is an arbitrary positive constant, if p_ε is sufficiently small, the third term of Equation (26) can be ignored, and Equation (26) becomes locally negative. From Assumption 2, the uncertainty Δ is assumed to be small, so ε is sufficiently small and the third term in Equation (26) can be ignored. Therefore, Equation (18) becomes a Lyapunov function if ε is sufficiently small, and ε can be minimized.

5.2. SMC with Uncertainty Compensation

The tracking error e^* with respect to the command value r of the ideal model is defined as shown in Equation (27).

$$e^*(t) = y^*(t)-r(t) \tag{27}$$

The dynamics of e^* are expressed as shown in Equations (3) and (28).

$$\begin{aligned}\ddot{e}^*(t) &= \ddot{y}^*(t)-\ddot{r}(t)\\ &= \frac{1}{m}(f_0(y^*,\dot{y}^*)(t)+f_u^*(t))-\ddot{r}(t)\end{aligned} \tag{28}$$

For these two variables, e and e^*, the sliding surface s is defined by using the constants $p_1, p_2, p_3, p_4, p_5 \in \mathbb{R}_+$, as shown in Equation (29).

$$s(t) = p_1e(t)+p_2\dot{e}(t)+p_3\ddot{e}(t)+p_4e^*(t)+p_5\dot{e}^*(t)+\ddot{e}^*(t) \tag{29}$$

For the switching surface s shown in Equation (29), the Lyapunov function V is defined as shown in Equation (30).

$$V(s) = \frac{K_1}{\gamma_1+1}|s|^{\gamma_1+1}+\frac{1}{2}\dot{s}^2 > 0 \tag{30}$$

where $0 < \gamma_1 \leq 1$ and $K_1 > 0$ are constants. The time derivative of V is represented as follows:

$$\dot{V}(s) = \dot{s}(K_1|s|^{\gamma_1}\mathrm{sign}(s) + \ddot{s}) \tag{31}$$

Let, f_u^* and f_u be determined as shown in Equations (32)–(34).

$$f_u^*(t) = p_3^{-1}m(-p_1e^*(t) - p_2\dot{e}^*(t)) - f_0(y^*, \dot{y}^*)(t) + m\ddot{r}(t) \tag{32}$$

$$f_u(t) = f_u^*(t) + m(-p_4e(t) - p_5\dot{e}(t)) - f_0(e, \dot{e})(t) - K^*\hat{\Delta}(t) - mf_q(t) \tag{33}$$

$$\ddot{f}_q(t) = K_1|s(t)|^{\gamma_1}\mathrm{sign}(s(t)) + \left(K_2 + \bar{\bar{\Delta}}\right)\mathrm{sign}(\dot{s}(t)) \tag{34}$$

where $0 < K^* < 1$ and $K_2 > 0$ are design parameters, $\bar{\bar{\Delta}} > 0$ is the upper limit of the absolute value of uncertainty $\ddot{\Delta}$, and $\hat{\Delta}$ is the estimated value of uncertainty.

By substituting Equations (32)–(34) into Equation (31), Equation (35) is expressed. Here, since $K^* < 1$, $\left|\ddot{\Delta}(t) - K^*\ddot{\hat{\Delta}}(t)\right| \leq \left|\ddot{\Delta}(t)\right|$ holds, and the absolute value is greater than the original value, so Equation (35) is expressed as Equation (36). Since Equation (36) holds, V is a Lyapunov function, and the asymptotic stability of the control system is guaranteed. Therefore, $e \to 0$ and $e^* \to 0$ are guaranteed, and the response of the ideal model and the actual system follows the command value r.

$$\dot{V}(s) = -K_2|\dot{s}| + \left(\left(\ddot{\Delta}(t) - K^*\ddot{\hat{\Delta}}(t)\right)\dot{s} - \bar{\bar{\Delta}}|\dot{s}|\right) \tag{35}$$

$$\leq -K_2|\dot{s}| + \left(\left|\ddot{\Delta}(t)\right| - \bar{\bar{\Delta}}\right)|\dot{s}| < 0 \tag{36}$$

In actual implementation, Equation (34) is transformed into Equation (37) to implement it for chattering removal. Through this implementation, chattering is suppressed by making the control input continuous.

$$\ddot{f}_q(t) = K_1|s(t)|^{\gamma_1}\mathrm{sign}(s(t)) + \left(K_2 + \bar{\bar{\Delta}}\right)|\dot{s}(t)|^{\gamma_2}\mathrm{sign}(\dot{s}(t)) \tag{37}$$

5.3. Shape Parameter Identification of Generalized Gaussian Kernel

In this section, the method of identifying the shape parameters from the observation information is explained. In the generalized Gaussian kernel, σ and γ exist as shape parameters. The $n-$th central moment $M^n(\cdot), n \in \mathbb{N}$ of the generalized Gaussian distribution is used for the identification of the shape parameters. $M^n(\cdot)$ is expressed as shown in Equation (38).

$$M^n(\boldsymbol{x}) = \sum_{i=1}^{N} x_i^n \tag{38}$$

In the case of the generalized Gaussian distribution, the even-order central moment $M^{2m}(\cdot), m \in \mathbb{N}$ is expressed as shown in Equation (39).

$$M^{2m}(\boldsymbol{x}) = \left\{\sigma^2\frac{\Gamma(1/\gamma)}{\Gamma(3/\gamma)}\right\}^m \frac{\Gamma((2m+1)/\gamma)}{\Gamma(1/\gamma)} \tag{39}$$

From this equation, kurtosis ϕ is expressed as shown in Equation (40).

$$\phi = \frac{M^4(\boldsymbol{x})}{(M^2(\boldsymbol{x}))^2} = \frac{\Gamma(5/\gamma)\Gamma(1/\gamma)}{(\Gamma(3/\gamma))^2} \tag{40}$$

From these equations, the evaluation function $J(\gamma)$ with respect to γ is defined as the difference between the observed value of kurtosis and the value calculated from γ, as shown in Equation (41).

$$J(\gamma) = \frac{1}{2}\left(\phi - \frac{\Gamma(1/\gamma)\Gamma(5/\gamma)}{\Gamma(3/\gamma)^2}\right)^2 \tag{41}$$

γ is updated by Equation (42) so that the evaluation function $J(\gamma)$ is monotonically decreased, where $\eta_\gamma > 0$ is the update gain, and $\Gamma'(\cdot)$ is the first-order derivative of the gamma function.

$$\left(\frac{\dot{1}}{\gamma}\right) = \eta_\gamma \frac{\Gamma(3/\gamma)^3\left(\phi - \frac{\Gamma(1/\gamma)\Gamma(5/\gamma)}{\Gamma(3/\gamma)^2}\right)}{\Gamma'(1/\gamma)\Gamma(3/\gamma)\Gamma(5/\gamma) + 5\Gamma(1/\gamma)\Gamma(3/\gamma)\Gamma'(5/\gamma) - 6\Gamma(1/\gamma)\Gamma'(3/\gamma)\Gamma(5/\gamma)} \tag{42}$$

By updating γ according to Equation (42), the updated equation of the evaluation function $J(\gamma)$ becomes Equation (43), and $J(\gamma)$ monotonically decreases, so the convergence of γ is guaranteed.

$$\dot{J}(\gamma) = -\eta_\gamma\left(\phi - \frac{\Gamma(1/\gamma)\Gamma(5/\gamma)}{\Gamma(3/\gamma)^2}\right)^2 = -2\eta_\gamma J(\gamma) < 0 \tag{43}$$

Summarizing the above, the following steps are performed for each control cycle for the identification of the shape parameters.

Step 1: Set the initial values of σ and γ.
Step 2: Observe the state variable x using the sensor.
Step 3: Calculate the 2nd and 4th central moments using Equation (39) when $m = 1, 2$.
Step 4: Calculate the kurtosis ϕ using Equation (40).
Step 5: Update σ as the square root of the 2nd moment.
Step 6: Update γ using Equation (42).

5.4. Summary of Proposed Method

Summarizing the above, a block diagram of the control system is shown in Figure 4, where C represents Equation (32), P represents Equation (1), P_n represents Equation (3), S represents Equations (33) and (37), and Adaption Law represents Equation (20) and Section 5.3.

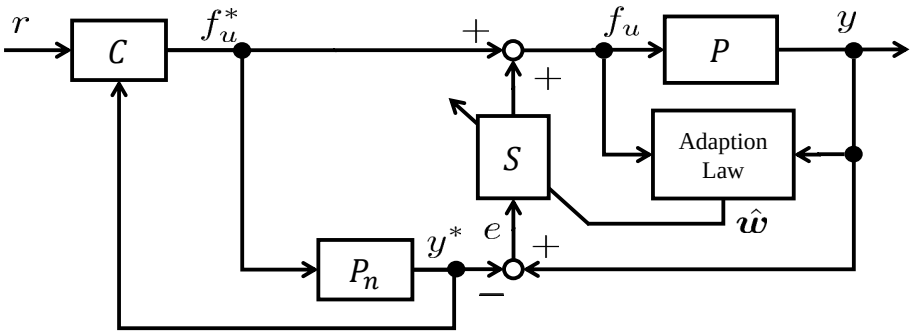

Figure 4. Control system of proposed method.

In actual program, the following steps are executed for each control cycle.

Step 1: Observe the stage position y using the sensor.
Step 2: Observe the stage velocity $\dot{y}$ by differentiating y.
Step 3: Update the shape parameters, σ and γ, according to the procedure in Section 5.3.
Step 4: Estimate the uncertainty $\hat{\Delta}$ using Equation (20). Here, the initial value of the state variable is 0, and v_1, v_2, and v_3 are the inputs to the observer, as shown in Equations (23)–(25).
Step 5: Calculate the ideal operation amount f_u^* using Equation (32).
Step 6: Calculate the actual operation amount f_u using Equations (33) and (37), and input it to the stage.

6. Verification

In this section, the proposed method is verified. The verification is divided into two parts: a simulation and an experiment.

The model of f_0 used in the verification is given by

$$f_0(y, \dot{y}) = -c\dot{y} - ky \tag{44}$$

where $c > 0$ and $k > 0$ are parameters set so that $f_0 \approx f$.

6.1. Simulation

A simulation of the proposed method was conducted. The simulation parameters are presented in Table 1, and the results are shown in Figure 5. Figure 5a–c show a comparison of the stage position, input voltage, and tracking error with and without uncertainty compensation. Figure 5d shows the magnitude of uncertainty with respect to the command force. The parameters were determined through trial and error. The reference value $r(t)$ is given by Equation (45). This is a sine wave with a frequency of 2 Hz and an amplitude of 1 mm.

$$r(t) = (1 - \cos(4\pi t)) \text{ [mm]} \tag{45}$$

In this simulation, Gaussian noise with a standard deviation of 1 was used for $\tilde{x}_i$.

Table 1. Simulation parameters.

Symbol	Value	Unit	Symbol	Value	Unit
m	0.0755	kg	p_1	625,000	–
c	0.105	kg/s	p_2	5000	–
k	2.5	kg/s^2	p_3	10	–
R	17.5	Ω	p_4	5,250,000	–
L	27.5×10^{-3}	H	p_5	5000	–
$\hat{a}$	31.7	N/A	K_1	500	–
$\hat{b}$	12.0	N/A	K_2	200	–
$\hat{k}$	100	/m	γ_1	0.8	–
L_x	0.01	m	γ_2	0.7	–
L_z	0.05	m	K^*	0.9	–
μ_f	6.3×10^{-3}	H/m	$\bar{\bar{\Delta}}$	100	N/s^2
μ_0	$4\pi \times 10^{-5}$	H/m	η_γ	0.1	–
l_y	0.05	m	σ	0.1	–
G_1	10	–	G_2	10	–
p_y	100	–	p_ε	7	–
N	100	–			

From the simulation results, it can be observed that perfect tracking is achieved with respect to the reference value, regardless of whether uncertainty compensation is applied or not. The effectiveness of perfect tracking control using sliding mode control is confirmed. Furthermore, the proposed method of uncertainty compensation reduces the tracking error compared to the case where no compensation is applied, demonstrating its effectiveness in achieving high-precision stage control. Additionally, it can be seen from Figure 5d that the uncertainty satisfies the assumptions in Section 3.

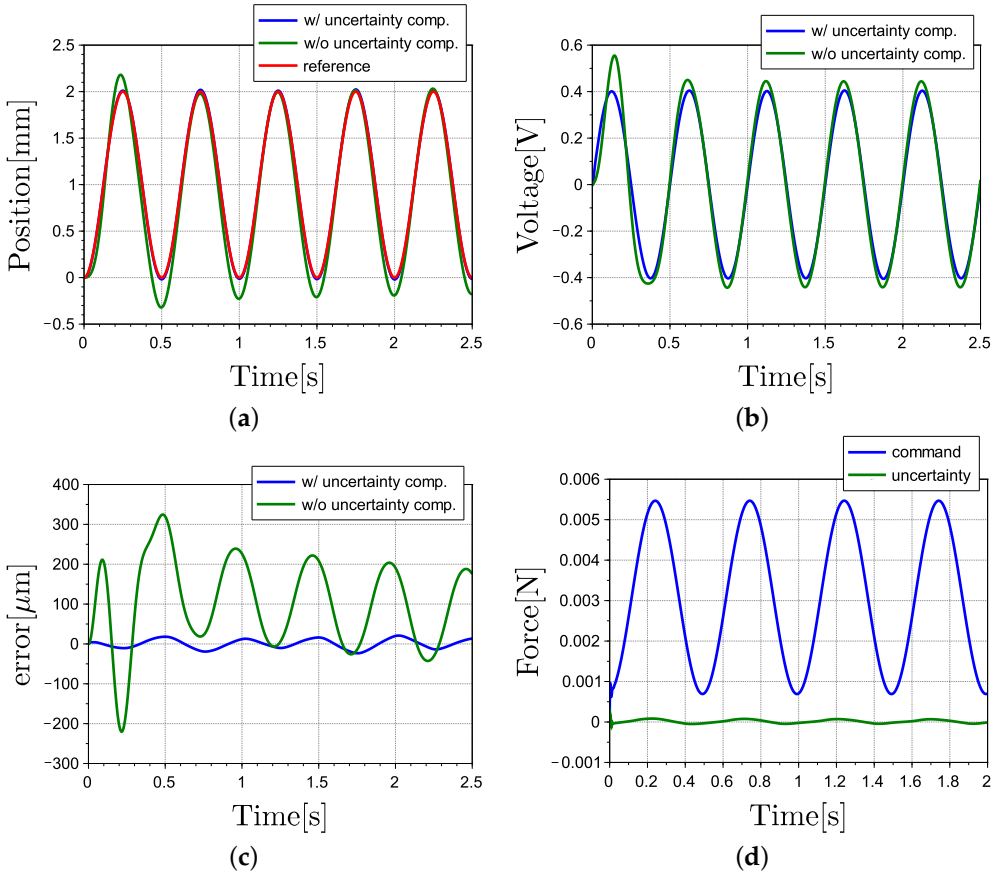

Figure 5. Simulation results: (**a**) stage position, (**b**) input voltage, (**c**) tracking error, (**d**) command force vs. uncertainty.

6.2. Experiment

An experiment was conducted on the designed control system. The same parameters as those used in the simulation were employed in the experiment. A sine wave with an amplitude of 1 mm and a frequency of 2 Hz was used as the command value r. The experimental results are presented in Figure 6. It can be seen from Figure 6d that the uncertainty is sufficiently small compared to the command force, and it satisfies the assumptions in Section 3. From Figure 6, it can be observed that without uncertainty compensation, sufficient tracking cannot be confirmed due to the uncertainties, and an error of up to 0.5 mm can be observed. However, by applying uncertainty compensation, it can be improved to within 0.2 mm at maximum. The effectiveness of the proposed method for uncertainty compensation is verified. However, it can be seen that higher-order vibrations occur in the proposed method. This is believed to be due to the fact that the uncertainty identifier picks up the sensor noise. Therefore, appropriately filtering the sensor value is a future task that can be performed to suppress higher-order vibrations.

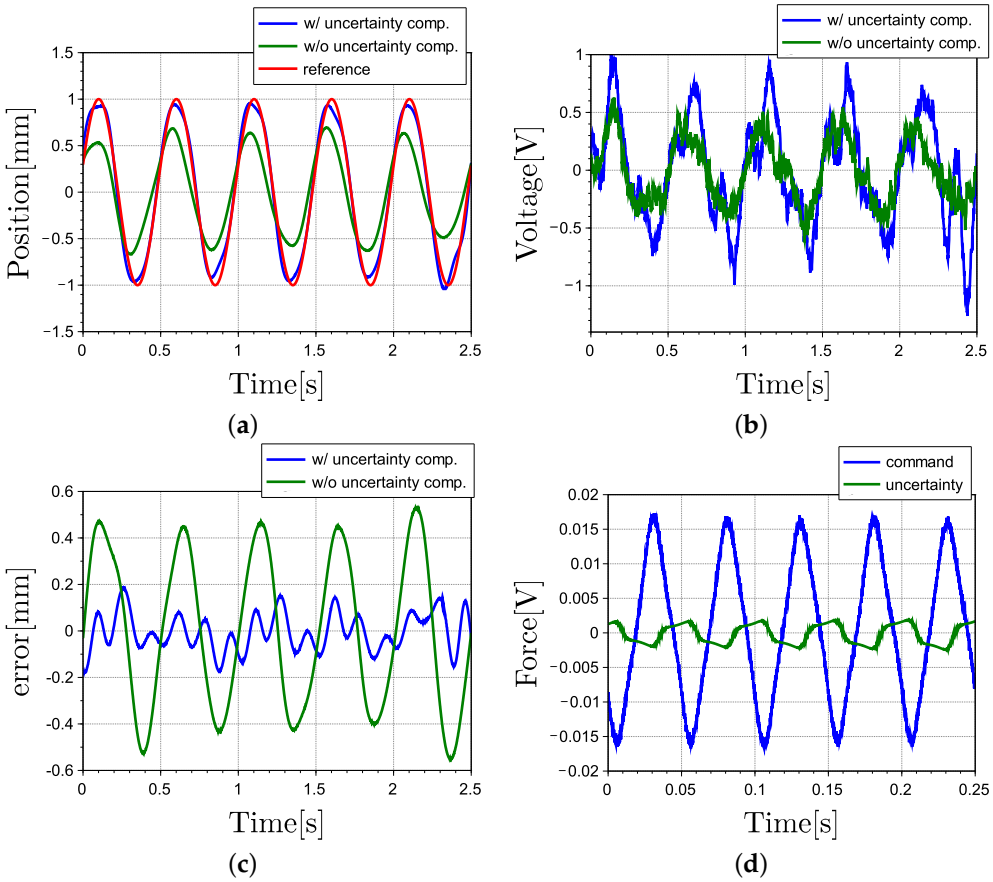

Figure 6. Experimental results: (**a**) position, (**b**) voltage, (**c**) error, (**d**) command force vs. uncertainty.

7. Conclusions

In this paper, we proposed a method to compensate for uncertainty using sliding mode control with an estimated uncertainty value, which represents the motion model of a linear slider as a linear operator and uncertainty. We designed a new observer using Kernel LMS for estimating uncertainty and succeeded in identifying uncertainty without directly observing it. By conducting experiments, we confirmed that it is possible to track the position of the stage even when the uncertainty is large in many cases. Specifically, under conditions that typically result in an error of about 0.5 mm using general sliding mode control, it was possible to reduce the error to about 0.2 mm using the proposed method.

Author Contributions: T.H. performed sliding mode control with uncertainty compensation and optimized the shape parameters. In addition, this paper was written.; T.Y. proposed the model of the linear motor. M.D. provided technical support and overall guidance for the paper. All authors have read and agreed to the published version of the manuscript.

Funding: This research received no external funding.

Data Availability Statement: Data are contained within the article.

Conflicts of Interest: The authors declare no conflict of interest.

References

1. Hsiao, H.H.; Wang, K.J. GAGAN: Global Attention Generative Adversarial Networks for Semiconductor Advanced Process Control. *IEEE Trans. Semicond. Manuf.* **2023**, *37*, 115–123. [CrossRef]
2. Kanarik, K.J.; Osowiecki, W.T.; Lu, Y.; Talukder, D.; Roschewsky, N.; Park, S.N.; Kamon, M.; Fried, D.M.; Gottscho, R.A. Human–machine collaboration for improving semiconductor process development. *Nature* **2023**, *616*, 707–711. [CrossRef]
3. Lee, C.Y.; Wu, C.M.; Hsu, C.Y.; Xie, H.H.; Fang, Y.H. Lithography reticle scheduling in semiconductor manufacturing. *Eng. Optim.* **2023**, 1–19. [CrossRef]

4. Malkin, A.; He, T. The geoeconomics of global semiconductor value chains: extraterritoriality and the US-China technology rivalry. *Rev. Int. Political Econ.* **2023** 1–26. [CrossRef]
5. Hager, A.; Güniat, L.; Morgan, N.; Ramanandan, S.P.; Rudra, A.; Piazza, V.; i Morral, A.F.; Dede, D. The implementation of thermal and UV nanoimprint lithography for selective area epitaxy. *Nanotechnology* **2023**, *34*, 445301. [CrossRef]
6. Fan, S.K.S.; Chen, M.S.; Hsu, C.Y.; Park, Y.J. An artificial intelligence transformation model–pod redesign of photomasks in semiconductor manufacturing. *J. Ind. Prod. Eng.* **2023**, 1–16. [CrossRef]
7. Sawlani, K.; Mesbah, A. Perspectives on artificial intelligence for plasma-assisted manufacturing in semiconductor industry. In *Artificial Intelligence in Manufacturing*; Academic Press: Cambridge, MA, USA, 2024; pp. 97–138.
8. Deng, M.; Iwai, Z.; Mizumoto, I. Robust parallel compensator design for output feedback stabilization of plants with structured uncertainty. *Syst. Control Lett.* **1999**, *36*, 193–198. [CrossRef]
9. Yang, G. Asymptotic tracking with novel integral robust schemes for mismatched uncertain nonlinear systems. *Int. J. Robust Nonlinear Control* **2023**, *33*, 1988–2002. [CrossRef]
10. Badings, T.; Romao, L.; Abate, A.; Parker, D.; Poonawala, H.A.; Stoelinga, M.; Jansen, N. Robust control for dynamical systems with non-gaussian noise via formal abstractions. *J. Artif. Intell. Res.* **2023**, *76*, 341–391. [CrossRef]
11. Gutiérrez-Oribio, D.; Tzortzopoulos, G.; Stefanou, I.; Plestan, F. Earthquake control: An emerging application for robust control. theory and experimental tests. *IEEE Trans. Control Syst. Technol.* **2023**, *31*, 1747–1761. [CrossRef]
12. Perrusquia, A.; Yu, W. Robust control under worst-case uncertainty for unknown nonlinear systems using modified reinforcement learning. *Int. J. Robust Nonlinear Control* **2020**, *30*, 2920–2936. [CrossRef]
13. Husain, S.S.; Kadhim, M.Q.; Al-Obaidi, A.S.M.; Hasan, A.F.; Humaidi, A.J.; Al Husaeni, D.N. Design of robust control for vehicle steer-by-wire system. *Indones. J. Sci. Technol.* **2023**, *8*, 197–216. [CrossRef]
14. Yoshida, R.; Tanigawa, Y.; Okajima, H.; Matsunaga, N. A design method of model error compensator for systems with polytopic-type uncertainty and disturbances. *SICE J. Control Meas. Syst. Integr.* **2021**, *14*, 119–127. [CrossRef]
15. Yang, C.; Xia, Y. Interval uncertainty-oriented optimal control method for spacecraft attitude control. *IEEE Trans. Aerosp. Electron. Syst.* **2023**, *59*, 5460–5471. [CrossRef]
16. Wang, X.; Chen, Z.; Yuan, Z. Output tracking based on extended observer for nonlinear uncertain systems. *arXiv* **2023**, arXiv:2302.05079.
17. Deng, M.; Inoue, A.; Zhu, Q. An integrated study procedure on real-time estimation of time-varying multi-joint human arm viscoelasticity. *Trans. Inst. Meas. Control* **2011**, *33*, 919–941. [CrossRef]
18. Jaeger, H. Adaptive nonlinear system identification with echo state networks. In *NIPS'02: Proceedings of the 15th International Conference on Neural Information Processing Systems*; MIT Press: Cambridge, MA, USA, 2002; Volume 15.
19. Glentis, G.O.; Berberidis, K.; Theodoridis, S. Efficient least squares adaptive algorithms for FIR transversal filtering. *IEEE Signal Process. Mag.* **1999**, *16*, 13–41. [CrossRef]
20. Hollweg, G.V.; Dias de Oliveira Evald, P.J.; Milbradt, D.M.C.; Tambara, R.V.; Gründling, H.A. Lyapunov stability analysis of discrete-time robust adaptive super-twisting sliding mode controller. *Int. J. Control* **2023**, *96*, 614–627. [CrossRef]
21. Abdelrhman, O.M.; Sen, L. Robust adaptive filtering algorithms based on the half-quadratic criterion. *Signal Process.* **2023**, *202*, 108775. [CrossRef]
22. Hoshina, T.; Deng, M. A Nonlinear Control of Linear Slider Considering Position Dependence of Interlinkage Flux. *Machines* **2022**, *10*, 522. . [CrossRef]
23. Deng, M.; Inoue, A.; Goto, S. Operator based Thermal Control of an Aluminum Plate with a Peltier Device. *Int. J. Innov. Comput. Inf. Control* **2008**, *4*, 3219–3229..
24. Gao, X.; Yang, Q.; Zhang, J. Multi-objective optimisation for operator-based robust nonlinear control design for wireless power transfer systems. *Int. J. Adv. Mechatron. Syst.* **2022**, *9*, 203–210. [CrossRef]
25. Bu, N.; Wang, X. Swing-up design of double inverted pendulum by using passive control method based on operator theory. *Int. J. Adv. Mechatron. Syst.* **2023**, *10*, 1–7. [CrossRef]
26. Bu, N.; Zhang, Y.; Zhang, Y.; Morohoshi, Y.; Deng, M. Robust Control for Hysteretic Micro-hand Actuator using Robust Right Coprime Factorization. *IEEE Trans. Autom. Control* **2023**, 1–7. [CrossRef]
27. Wang, Z.; Zhou, R.; Hu, C.; Zhu, Y. Online Iterative Learning Compensation Method Based on Model Prediction for Trajectory Tracking Control Systems. *IEEE Trans. Ind. Inform.* **2022**, *18*, 415–425. [CrossRef]
28. Li, Y.; Luo, P.; Peng, Y.; Liu, Z. Model Free iterative learning for table motion control of lithography machine. In Proceedings of the 2023 8th International Conference on Information Systems Engineering (ICISE), Dalian, China, 23–25 June 2023; pp. 47–50.
29. Ohnishi, W.; Strijbosch, N.; Oomen, T. State-tracking iterative learning control in frequency domain design for improved intersample behavior. *Int. J. Robust Nonlinear Control* **2023**, *33*, 4009–4027. [CrossRef]
30. Ishii, H.; Manabe, T.; Wakui, S. Reinterpretation of PDD2 compensator embedded in position control for pneumatic stage. *J. Adv. Mech. Des. Syst. Manuf.* **2019**, *13*, JAMDSM0074. [CrossRef]
31. Saito, D.; Wakui, S. Trial of applying the unbalance vibration compensator to axial position of the rotor with AMB. In Proceedings of the 2017 International Conference on Advanced Mechatronic Systems (ICAMechS), Xiamen, China, 6–9 December 2017; pp. 249–254.
32. Dhavalikar, M.; Dingare, S.; Patle, B. Prediction of Positioning Accuracy and Settling Time of Double Acting Single Rod Pneumatic Cylinder Using SIMULINK. *Int. J. COMADEM* **2024**, *27*, 25–29.

33. Liu, W.; Pokharel, P.P.; Principe, J.C. The kernel least-mean-square algorithm. *IEEE Trans. Signal Process.* **2008**, *56*, 543–554. [CrossRef]
34. Yu, X.; Feng, Y.; Man, Z. Terminal sliding mode control–an overview. *IEEE Open J. Ind. Electron. Soc.* **2020**, *2*, 36–52. [CrossRef]
35. Shtessel, Y.; Edwards, C.; Fridman, L.; Levant, A. *Sliding Mode Control and Observation*; Springer: New York, NY, USA, 2014; Volume 10.
36. Levant, A. Sliding order and sliding accuracy in sliding mode control. *Int. J. Control* **1993**, *58*, 1247–1263. [CrossRef]
37. Zhihong, M.; Paplinski, A.P.; Wu, H.R. A robust MIMO terminal sliding mode control scheme for rigid robotic manipulators. *IEEE Trans. Autom. Control* **1994**, *39*, 2464–2469. [CrossRef]
38. Zhao, H.; Xiang, W.; Lv, S. A variable parameter LMS algorithm based on generalized maximum correntropy criterion for graph signal processing. *IEEE Trans. Signal Inf. Process. Netw.* **2023**, *9*, 140–151. [CrossRef]
39. Chen, Z.; Wang, C.; Wang, H.; Ma, Y.; Liang, G.; Wu, X. Heterogeneous Sensor Information Fusion based on Kernel Adaptive Filtering for UAVs' Localization. In Proceedings of the 2017 IEEE International Conference on Information and Automation (ICIA), Macao, China, 18–20 July 2017; pp. 171–176. . [CrossRef]
40. Xiao, Y.; Yan, W.; Doğançay, K.; Ni, H.; Wang, W. Multikernel adaptive filtering over graphs based on normalized LMS algorithm. *Signal Process.* **2024**, *214*, 109230. [CrossRef]
41. Shi, L.; Lu, R.; Liu, Z.; Yin, J.; Chen, Y.; Wang, J.; Lu, L. An Improved Robust Kernel Adaptive Filtering Method for Time Series Prediction. *IEEE Sens. J.* **2023**, *23*, 21463–21473. [CrossRef]
42. Meng, L.; Hirayama, T.; Oyanagi, S. Underwater-drone with panoramic camera for automatic fish recognition based on deep learning. *IEEE Access* **2018**, *6*, 17880–17886. [CrossRef]
43. Bi, S.; Qu, X.; Ma, L.; Shen, T.; Han, C. Apple grading method based on ordered partition neural network. In Proceedings of the 2021 International Conference on Advanced Mechatronic Systems (ICAMechS), Tokyo, Japan, 9–12 December 2021; pp. 200–205.
44. Zhao, Y.; Niu, B.; Zong, G.; Zhao, X.; Alharbi, K.H. Neural network-based adaptive optimal containment control for non-affine nonlinear multi-agent systems within an identifier-actor-critic framework. *J. Frankl. Inst.* **2023**, *360*, 8118–8143. [CrossRef]
45. Kurani, A.; Doshi, P.; Vakharia, A.; Shah, M. A comprehensive comparative study of artificial neural network (ANN) and support vector machines (SVM) on stock forecasting. *Ann. Data Sci.* **2023**, *10*, 183–208. [CrossRef]
46. Huang, F.; Xiong, H.; Chen, S.; Lv, Z.; Huang, J.; Chang, Z.; Catani, F. Slope stability prediction based on a long short-term memory neural network: Comparisons with convolutional neural networks, support vector machines and random forest models. *Int. J. Coal Sci. Technol.* **2023**, *10*, 18. [CrossRef]
47. Mahesh, P.V.; Meyyappan, S.; Alla, R. Support Vector Regression Machine Learning based Maximum Power Point Tracking for Solar Photovoltaic systems. *Int. J. Electr. Comput. Eng. Syst.* **2023**, *14*, 100–108.
48. Labbadi, M.; Cherkaoui, M. Robust adaptive nonsingular fast terminal sliding-mode tracking control for an uncertain quadrotor UAV subjected to disturbances. *ISA Trans.* **2020**, *99*, 290–304. [CrossRef]
49. Diana, D.; Carline, M.J. Hybrid metaheuristic method of ABC kernel filtering for nonlinear acoustic echo cancellation. *Appl. Acoust.* **2023**, *210*, 109443. [CrossRef]
50. Novey, M.; Adali, T.; Roy, A. A complex generalized Gaussian distribution—Characterization, generation, and estimation. *IEEE Trans. Signal Process.* **2009**, *58*, 1427–1433. [CrossRef]
51. Deng, M.; Wen, S.; Inoue, A. Sensorless anti-swing robust nonlinear control for travelling crane system using SVR with generalized Gaussian function and robust right coprime factorization. *Trans. Soc. Instrum. Control Eng.* **2011**, *47*, 366–373. [CrossRef]

Disclaimer/Publisher's Note: The statements, opinions and data contained in all publications are solely those of the individual author(s) and contributor(s) and not of MDPI and/or the editor(s). MDPI and/or the editor(s) disclaim responsibility for any injury to people or property resulting from any ideas, methods, instructions or products referred to in the content.